Development of steady-state operation using ion cyclotron heating in the Large Helical Device

メタデータ	言語: English 出版者: 公開日: 2015-04-21 キーワード (Ja): キーワード (En): 作成者: Kasahara, H., Seki, T., Saito, K., Seki, R., Kumazawa, R., Yoshimura, Y., Kubo, S., Shimozuma, T., Igami, H., Takahashi, H., Nagasaki, K., Ueda, Y., Tokitani, M., Ashikawa, N., Shoji, M., Wakatsuki, T., Kamio, S., Tsuchiya, H., Yoshimura, S., Tamura, N., Suzuki, C., Yamada, H., Muto, T., LHD, Experiment Group メールアドレス: 所属:
URL	http://hdl.handle.net/10655/12476

This work is licensed under a Creative Commons Attribution-NonCommercial-ShareAlike 3.0 International License.

Physics of Plasmas

Development of steady-state operation using ion cyclotron heating in the Large Helical Device

Cite as: Phys. Plasmas **21**, 061505 (2014); https://doi.org/10.1063/1.4884363
Submitted: 26 January 2014 • Accepted: 10 May 2014 • Published Online: 19 June 2014

H. Kasahara, T. Seki, K. Saito, et al.

View Online Export Citation CrossMark

ARTICLES YOU MAY BE INTERESTED IN

Fast ion charge exchange spectroscopy measurement using a radially injected neutral beam on the large helical device
Review of Scientific Instruments **79**, 10E519 (2008); https://doi.org/10.1063/1.2968695

Performance of the newly installed vertical neutron cameras for low neutron yield discharges in the Large Helical Device
Review of Scientific Instruments **91**, 083505 (2020); https://doi.org/10.1063/5.0010302

Physics and applications of three-ion ICRF scenarios for fusion research
Physics of Plasmas **28**, 020501 (2021); https://doi.org/10.1063/5.0021818

© 2014 AIP Publishing LLC.

Development of steady-state operation using ion cyclotron heating in the Large Helical Device

H. Kasahara,[1] T. Seki,[1] K. Saito,[1] R. Seki,[1] R. Kumazawa,[1] Y. Yoshimura,[1] S. Kubo,[1] T. Shimozuma,[1] H. Igami,[1] H. Takahashi,[1] K. Nagasaki,[2] Y. Ueda,[3] M. Tokitani,[1] N. Ashikawa,[1] M. Shoji,[1] T. Wakatsuki,[4] S. Kamio,[1] H. Tsuchiya,[1] S. Yoshimura,[1] N. Tamura,[1] C. Suzuki,[1] H. Yamada,[1] T. Mutoh,[1] and LHD Experiment Group
[1]*National Institute for Fusion Science, Toki, Japan*
[2]*Institute of Advanced Energy, Kyoto University, Uji, Japan*
[3]*Osaka University, Suita, Japan*
[4]*The University of Tokyo, Kashiwa, Japan*

(Received 26 January 2014; accepted 10 May 2014; published online 19 June 2014)

Using a handshake shape (HAS) antenna phasing dipole for ion cyclotron heating (ICH), the heating efficiency was higher than that using a previous poloidal array antenna in the Large Helical Device. In order to sustain the dipole operation, real-time feedback for impedance matching and maintaining the same phase and power was adopted during long-pulse discharge. The HAS antenna was designed to reduce parasitic losses associated with energetic particle and radio-frequency (RF) sheath effects by field-aligned current concentration on the midplane. Local hot spots and the inhomogeneity of the diverter heat profile in the toroidal direction were reduced. The long-pulse discharge with an electron density (n_{e0}) of 1×10^{19} m^{-3}, center electron temperature (T_{e0}) of 2.5 keV, a plasma duration time (t_d) of 19 min, and RF heating power (P_{RF}) of 1 MW was achieved by ICH and electron cyclotron heating. © *2014 AIP Publishing LLC*. [http://dx.doi.org/10.1063/1.4884363]

I. INTRODUCTION

In designing a commercial fusion reactor, steady-state operation is important to decrease the cost of electricity and to increase the lifetime of the fusion plant. Fast-wave heating in the ion cyclotron range of frequencies (ICRF) has been performed for steady-state discharges in the Large Helical Device (LHD).[1] A long-pulse discharge with the plasma duration time (τ_d) of 54 min was demonstrated with the line-averaged electron density (n_e) of 0.4×10^{19} m^{-3}, the central electron temperature (T_{e0}) of 1 keV, and the radio-frequency (RF) heating power (P_{RF}) of 0.5 MW (electron cyclotron heating (ECH): 0.1 MW, ion cyclotron heating (ICH): 0.4 MW) in a hydrogen-minority heating regime with helium plasmas.[2] As plasma duration time and RF heating power increase, hot spots and sparks appear at various places inside of the vacuum vessel. With the persistence of strong hot spots and increasing frequencies of flashes, long-pulse discharges are usually terminated by an unpredicted radiation collapse within a time scale of 0.2 s.[3] In the end of the plasma, the intensity of the iron line spectrum first arises, and then electron temperature at the plasma edge begins to drop before the radiation collapse. In order to understand the mechanism of the penetration and production for impurities, toroidal phasing experiments for ICH have been conducted to decrease the impurity production associated with RF sheath potential and energetic particles at the plasma edge with a dipole phase in the LHD.

In this paper, typical design parameters of two kinds of ICRF antennas, a handshake shape (HAS) antenna[4] and a poloidal array (PA) antenna, are described in Sec. II, and initial experiment results for the reduction of local hot spots and the improvement of a toroidal phasing system with real-time feedback controls are shown in Sec. III. Finally, we discuss the critical issues faced in a long-pulse discharge with a τ_d of 19 min in steady-state operation with a helium plasma and the improvements of ICH using the HAS antenna.

II. ICRF ANTENNA IN LHD

The previous long-pulse discharge with a τ_d of 54 min was demonstrated by ICH + ECH on a hydrogen-minority heating regime for a helium plasma with the magnetic field (B_t) of 2.712 T on the magnetic axis (R_{ax}) of 3.65 m, and ICH was carried out only by using the PA antenna shown in Fig. 1(a). A magnetic axis sweeping from $R_{ax} = 3.63$ m to $R_{ax} = 3.67$ m every 3 min, the time-averaged heat flux to the

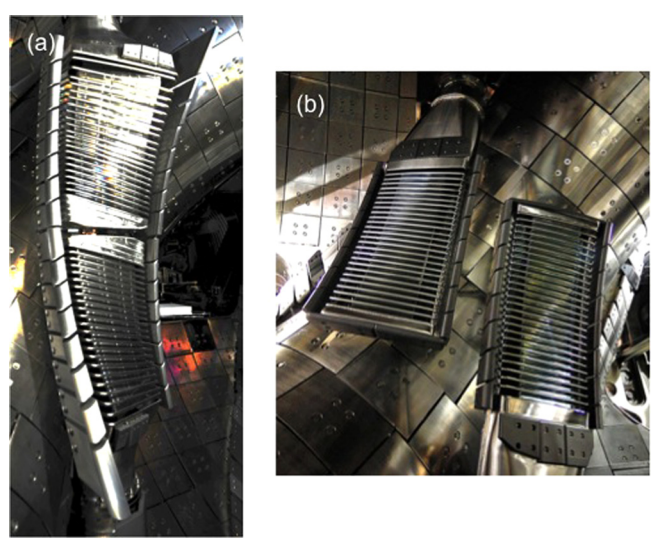

FIG. 1. Picture of two kinds of ICRF antennas installed in the LHD. The left figure (a) shows the poloidal PA at the 7.5 port, and the right figure (b) shows the HAS antenna at the 3.5 port. Magnetic field lines in front of ICRF antennas are aligned to a FS.

 © 2014 AIP Publishing LLC

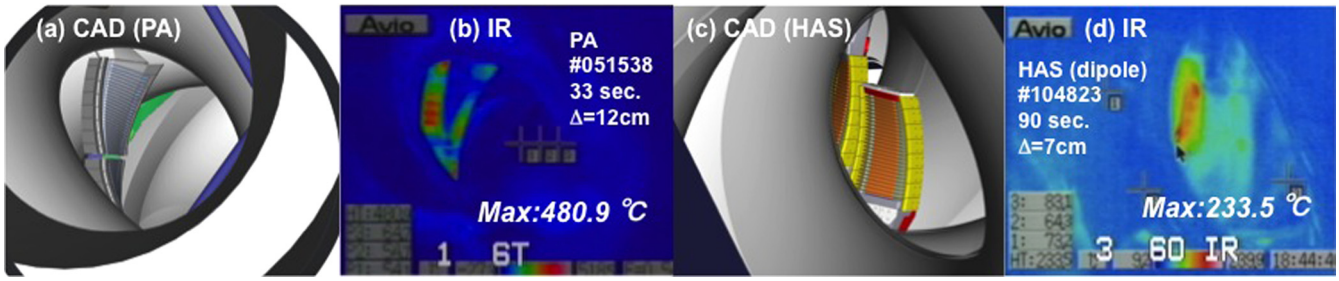

FIG. 2. Pictures of the HAS and the PA antenna installed in the vacuum vessel in Figs. 3(a) and 3(c), and the local hot spot temperatures measured by IR camera around ICRF antennas on the long-pulse discharges are shown in Figs. 3(b) and 3(d). The temperatures of local hot spots using the PA were approximately twice those using the HAS at the heating power of 0.6 MW for ICH, and the distance Δ using the HAS antenna between the Faraday screen and LCFS was shorter than that for the PA antenna.

divertor plates was alternately scattered to the inner-side and the outer-side divertor plates.[5] The magnetic axis sweeping decreased the frequency of flash events, but it was necessary to decrease the heating power for ICH to maintain long-pulse plasma duration with a low frequency of flashes inside the vacuum vessel. In order to sustain plasmas of higher electron density ($n_e \sim 1 \times 10^{19}\ \mathrm{m}^{-3}$), it is necessary to increase RF heating power, but the ICH heating power seems to be strongly related to the frequency of flashes.[6] In previous works to decrease impurity generation during ICH, a low-Z coating on plasma-facing components,[7] reducing the sheath potential by the antenna phase,[8] decreasing the inductive imaginary current on the Faraday screen (FS) caused by misalignment[9] and rotating the center conductor[10] to a magnetic field line (MFL) have been attempted, and a favorable ICH with low impurity generation and relatively high heating efficiency was achieved with a phasing dipole.[11–14] It has been reported that field alignment for the ICRF antenna should theoretically decrease the average RF sheath potential along magnetic field lines in the Alcator C-Mod,[15] and that low-impurity production is achieved by dipole phasing using a field-aligned ICRF antenna.[16] In steady-state operation, dipole phasing may, indeed, be one of the candidate methods for decreasing impurity generation during ICH, and a toroidal phasing experiment was planned to execute a stable steady-state plasma using a field-aligned ICRF antenna in the LHD. In the Alcator C-Mod, the fast wave is excited using 4 (toroidal direction) × 2 (poloidal direction) antennas within the narrow-peak toroidal wavenumber spectrum with dipole phasing, and the fast wave is excited using 2 (toroidal direction) antenna with the peak toroidal wavenumber on a large-magnetic-field configuration rather than the magnetic field at the plasma center in the LHD. The field-aligned toroidal phasing antenna in the LHD, i.e., the HAS antenna, was designed to decrease impurity generation and local hot-spots temperatures associated with the RF sheath; using this system, fast wave heating experiments in various toroidal phases have been investigated since 2009.

A. Experimental setup for two kinds of ICRF antennas

Two kinds of ICRF antennas, the PA antenna in Fig. 1(a) and the HAS antenna in Fig. 1(b), were installed in different toroidal sections, and the toroidal angle between these antennas is 144°. The PA antenna was installed perpendicular to the equatorial plane at port 7.5, and the tilt angle of the FS of the PA antenna to the equatorial plane is approximately 12°. The center conductor (strap) of the PA antenna is tilted to magnetic field line, and the strap of the HAS antenna at port 3.5 is aligned with the line. The strap of the HAS antenna is ideally installed to the vertical magnetic field line, and then the excited waves driven by the image current to cancel the parallel RF electric field $E_{\parallel}$ are smaller than that using the PA antenna. The RF current on the strap surface beside the plasma is strongly concentrated on both strap edges, and the maximum of the RF current is close to the bottom plate of the HAS antenna.[1] For the HAS antenna, the decreasing the temperature of local hot spots and decreasing impurity contamination are two important issues, and the RF current of both straps is concentrated on the mid plane to decrease the RF sheath potential caused by mismatched amplitude for excited waves for the HAS antenna around regions with large RF current concentrations (Fig. 2).

Typical antenna parameters and operational conditions in steady-state operation are shown on Table I. The strap width and the distance (Δ_{LCFS}) between the strap and the last closed flux surface (LCFS) in front of ICRF antennas were smaller for the HAS antenna than the PA antenna, because the vacuum loading of the HAS antenna was smaller than that of the PA antenna at the same Δ_{LCFS}. On previous steady-state operation (~54 min), the local hot spot temperature of the antenna protector edge using the PA antenna was over 1000 °C with a Δ_{LCFS} of 12 cm and the heating power of 0.4 MW for ICH, and it was necessary to both decrease the local hot spot temperature and increase the heating power for higher-density operation. In order to increase the cooling capability of the antenna protector, the material of the protector was changed from a isotropic carbon (IG-43) to a carbon-fiber composite (CX-2002), and the heat conductivity for the CX-2002 in the direction of the cooling water was three times higher than that for the IG-43. An effective excited spectrum of parallel wavenumber ($k_{\parallel}$) to the magnetic field line using the HAS antenna in dipole phase was larger than that using the PA antenna in monopole phase. The effective spectrum of $k_{\parallel}$ for the HAS antenna was approximately $\sim 7\ \mathrm{m}^{-1}$, and that of the PA antenna was $\sim 0\ \mathrm{m}^{-1}$ with a weak large-wavenumber spectrum caused by the strap width. Since the perpendicular refractive index (n_{perp}) in fast wave is a function of the electron density, the magnetic field and the parallel refractive index, the

TABLE I. Typical design parameters for the PA and the HAS antenna. The angle of the MFL around the ICRF antenna is tilted at 12° to the equatorial plane. The PA antenna is installed perpendicular to the plane, and the installation angle of the HAS antenna is ∼78° to the plane. The main material of the antenna is SUS316, but the antenna protector was made with low-Z material (carbon).

	PA	HAS
Installation angle of strap to MFL	90 deg (not field-aligned)	78 deg (field-aligned)
Strap width/length (m)	0.3/0.7	0.2/0.7
Strap—FS	0.04/0.01	0.05/0.015
Parallel/vertical (m)	0.09	0.05
Strap—backplate (m)	$\sim 0\,\mathrm{m}^{-1}$ ($\eta > 70\%$)	$\sim 7\,\mathrm{m}^{-1}$ (dipole, $\eta > 90\%$), $\sim 0\,\mathrm{m}^{-1}$ (monopole, $\eta > 70\%$)
Typical wavenumber $k_{\parallel}$ (m^{-1}) and heating efficiency (η)	IG-43 (isotropic carbon)	
Material of antenna protector		CX-2002 (carbon fiber composite)

propagating region for fast waves with large $k_{\parallel}$ values ($\sim 7\,\mathrm{m}^{-1}$) is shifted by a few cm to a higher-density region than that with the lower $k_{\parallel}$ ($\sim 0\,\mathrm{m}^{-1}$) for the PA antenna. Due to this shift in the wave propagation region, the possibility of plasma edge damping seems to be smaller for the HAS antenna than for the PA antenna. It was assumed that the heating efficiency (η) for the HAS with dipole phase was higher than that for the PA antenna with monopole phase, and in the initial fast wave heating experiment, this was consistent with the experimental results, shown in Table I.

III. STEADY-STATE EXPERIMENTS USING ICH

A. Local hot spots using the PA and the HAS antennas

Figure 3 shows two pictures for the PA and the HAS antenna made by a computer-aided designed system (CAD) and local hot-spot temperatures around ICRF antennas on long-pulse operations. The ICH heating powers ($P_{\mathrm{ICH}} \sim 0.6\,\mathrm{MW}$) at the frequency of 38.47 MHz were approximately the same, and the antenna distances ($\Delta_{\mathrm{LCFS}} \sim 7\,\mathrm{cm}$) for the HAS with the dipole phase was closer than that for the PA ($\Delta_{LCFS} \sim 12\,\mathrm{cm}$). An infrared (IR) camera measured the local hot-spot temperatures, and the temperature of the PA antenna protector was increased with increased plasma duration. The maximum temperature reached using the PA antenna was 480 °C after 33 s while that of the HAS antenna was 234 °C after 90 s. The hot spot region of the antenna protector for the PA antenna was close to the divertor leg with the large curvature, and the predicted geometrical misalignment for the divertor leg might be one of the causes of the hot spots. In the present work, tracking energetic particles accelerated on the ICRF resonance between the ICRF antenna and LCFS, the energetic particles easily impacted the upper edge of the antenna protector of the PA antenna, and the impact region was consistent with hot spots found in a previous experimental observation.[3] On the other hand, the region of local hot spots for the HAS antenna was broader and located around the region geometrically closest to the minimum of Δ_{LCFS}, and this region for the HAS antenna was not strongly related to direct energetic particle losses during ICH. These results suggest that the local heat load using the HAS antenna is decreased with the improvement of heat conductivity using the carbon-fiber-composite and the reduction of parasitic losses associated with the energetic particles in front of the ICRF antenna. Since there is no installation to measure the RF sheath potential around these ICRF antennas in the LHD, an actual antenna model has been prepared by a collaboration between NIFS and PSFC (MIT)[15,17,18] using a finite element solver, COMSOL.[19] The initial result with the cold plasma tensor of the LHD and without the model for Faraday screen and antenna protectors has already been found, but it is necessary

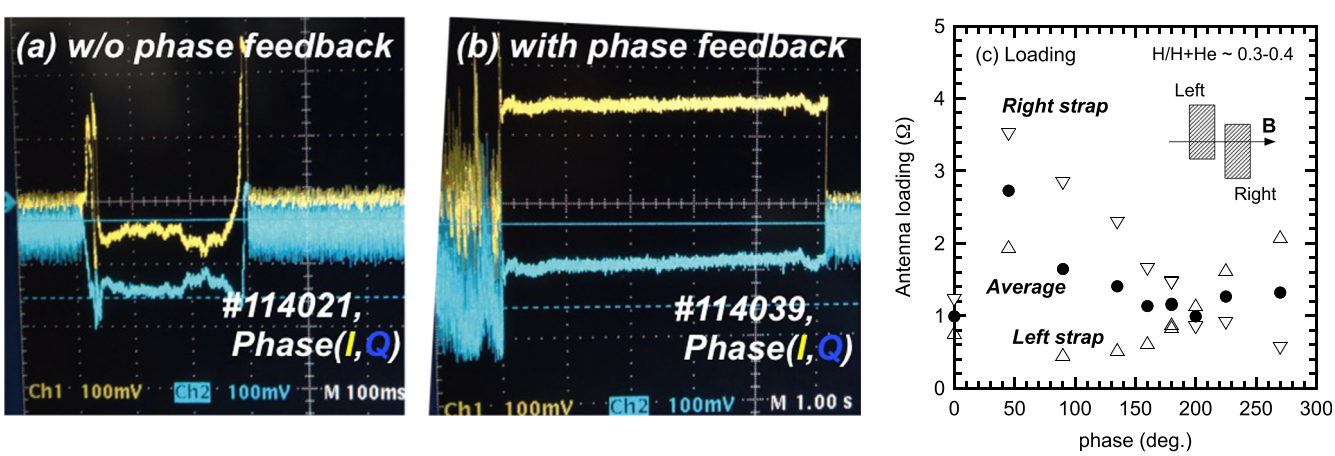

FIG. 3. In-phase (I) and quadrature-phase (Q) between two transmission lines associated with the strap surface current of the HAS antenna are shown in Figs. 4(a) and 4(b), with the phase of the current strap kept constant by a real-time phase feedback control during discharge, shown in Fig. 4(b). Figure 4(c) shows the average antenna loading during 10 s in various antenna phases on the hydrogen minority heating regime with the ratio over than 30%, and the difference of antenna loading between the two straps for the HAS antenna was small in the monopole (0–0) and dipole (0–180) phases.

to improve the optimization of the calculation mesh on the plasma surface and decrease the calculation resources needed to include the Faraday screen and the antenna protectors.

B. Real-time phase feedback control for long-pulse operation

In order to increase the heating efficiency and decrease the temperature of local hot spots during dipole-phase ICH using the HAS at steady-state operation, it is necessary to maintain the same antenna phase during long-pulse operation in real time, because it has been reported that the antenna impedance for the PA antenna is gradually changed during long-pulse operation.[20,21] Since the antenna loadings for the PA antenna were not sensitive to various antenna phases, it was not an important issue to control the antenna phase for the PA antenna in real time for long-pulse operation. Figures 3(a) and 3(b) show the experimental results for the in-phase (I) and the quadrature-phase (Q) between two transmission lines associated with the antenna phase for the HAS antenna with and without real-time phase feedback control. On short-pulse discharge (~0.3 s) without the real-time phase feedback control in Fig. 3(a), the I- and the Q-phase did not keep constant, but rather depended on plasma parameters. The plasma was sustained by electron cyclotron heating (ECH) and ICH, and the end of the plasma duration in the last 0.1 s was only sustained by ICH. At that time, the electron temperature decreased, and the phase clearly changed. This result suggests that there is no guarantee of maintaining the same phase for the HAS antenna at various plasma parameters. For steady-state operation, real-time impedance matching is needed to make the RF reflection ratio small,[20] and phase feedback control has to be carried out simultaneously with other feedback controls like impedance matching and maintenance of the power level. The initial result for real-time phase feedback control was demonstrated at a duration of 5 s in Fig. 3(b), and the I- and Q-phases for the current strap were kept constant during the discharges. The maximum speed of phase control was less than 36°/s, which was not a limiting factor; rather, the speed was limited by the speed of impedance matching for a liquid stub tuner[21] with a low power-reflection ratio.

Using real-time phase feedback control, the antenna loading of the HAS antenna is shown in various toroidal phases with the duration time of 10 s on the hydrogen minority heating regime in Fig. 3(c), although the hydrogen minority ratios between 0.3 and 0.4 were not optimized in these experiments. Unbalanced antenna-loadings were clearly increased except in dipole or monopole phases, and the maximum imbalance in antenna loading was achieved at a phase of 90°. The antenna loading with phasing monopole was slightly larger than the antenna loading with phasing dipole, and it differed from the assumption before the experiment. The antenna loading with monopole phasing was much larger than that with dipole phasing. This may be one of the reasons for the imaginary current on the surface for the support of each HAS antenna protector, making the antenna loading small at the monopole phase.

C. Higher performance steady-state discharge

High-performance long-pulse discharge with τ_d of 19 min, n_e of $10^{19}\,m^{-3}$, and T_{e0} of 2.5 keV was achieved using the HAS and the PA antennas with several real-time feedback controls during steady-state operation, and various plasma parameters are shown in Fig. 4. For ECH, one focused on off-axis heating with frequency (f_{req}) of 84 GHz and two focused on on-axis heating with f_{req} of 77 GHz were used, and the on-axis heatings ($f_{req} \sim 77$ GHz) were injected in a series at 120-s intervals in different toroidal sections to decrease the internal pressure of the ECH gyrotron. The center electron temperature (T_e) was measured by electron cyclotron emission (ECE) in Fig. 4(b), and the T_e strongly

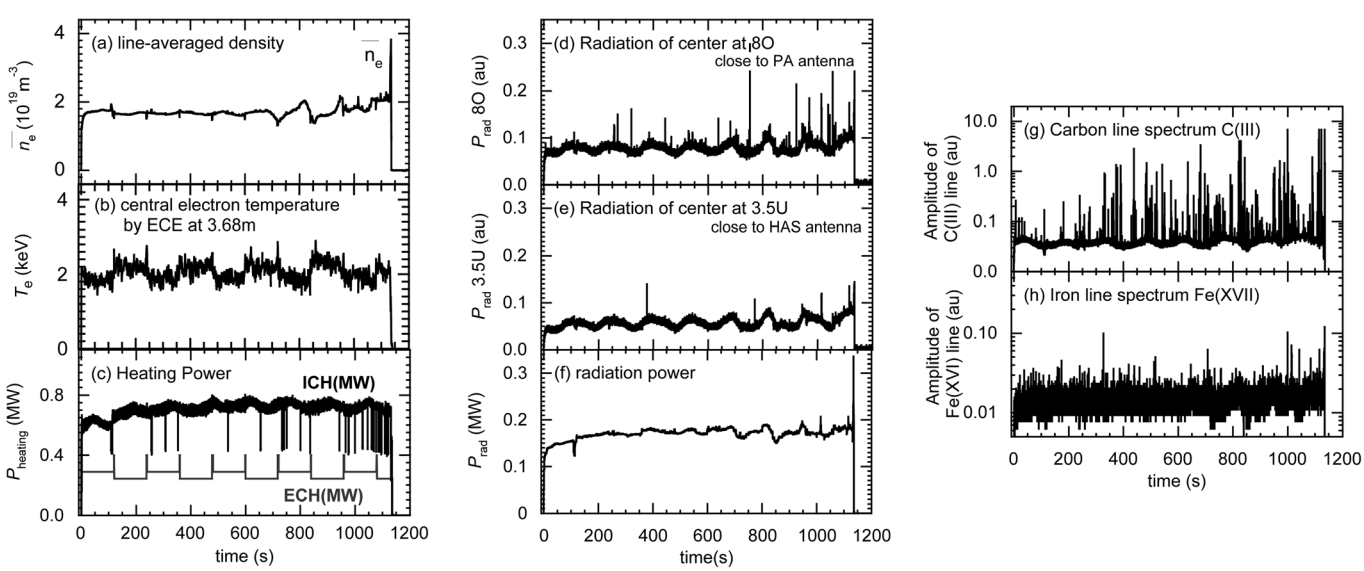

FIG. 4. Discharge waveform for higher-performance steady-state discharge with n_e of $10^{19}\,m^{-3}$ an T_{e0} of 2.5 keV and P_{RF} of 1 MW (ICH: 0.72 MW, ECH: 0.26 MW). The radiation P_{rad} measured by bolometer was less than 20% during the discharge. The magnetic axis was swept from $R_{ax} = 3.63$ m to $R_{ax} = 3.67$ m with $B_t = 2.71$ T on $R_{ax} = 3.65$ m to scatter the local divertor heat load.

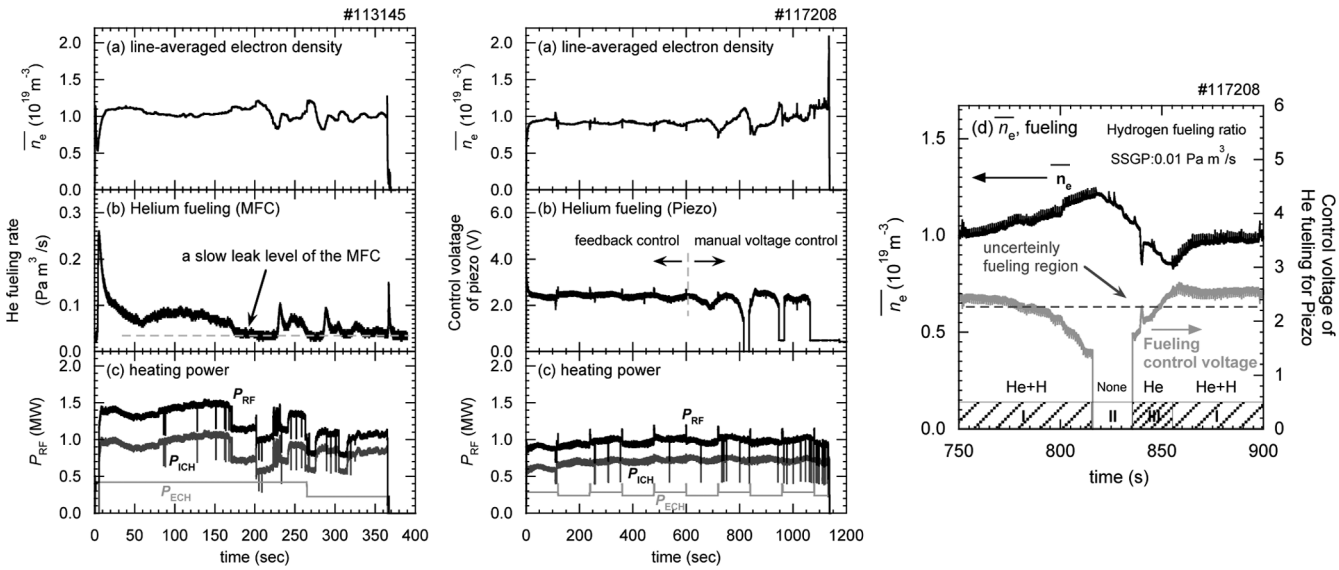

FIG. 5. The particle fueling rate of He was measured by MFC for the long-pulse plasma with $\tau_d \sim 6$ min and n_e of 1×10^{19} m^{-3} (#113145) and are shown at the left figure in Fig. 5, and the control voltage of particle fueling using piezoelectric valve are shown in steady-state plasma with $\tau_d \sim 19$ min, $n_e \sim 1 \times 10^{19}$ m^{-3} and $P_{RF} \sim 1$ MW (#117208) in the middle figure. In the preliminary estimation for particle fueling using a piezoelectric valve, the particle-fueling rate decreased to 0.01 Pa m^3/s from 2 Pa m^3/s at 700 s. Hydrogen fueling was effectively decreased in flashes inside of vacuum vessel using the PA antenna, the hydrogen was SSGP, which was installed just in front of the HAS antenna, with the hydrogen fueling rate <0.01 Pa m^3/s.

depended on the on-axis heating. Total radiation power (P_{rad}) was measured by the bolometer installed in port 3.5 close to the HAS antenna. The P_{rad} was affected by the time evolution of T_e, and it was kept constant ($P_{rad} < 0.2$ MW). As the plasma duration with $n_e \sim 1 \times 10^{19}$ m^{-3} and T_e greater than a few keV was extended, a large amount of spikes indicating impurity lines (CIII and FeXVI) and fast radiation powers in Figs. 4(d) and 4(e) located in different toroidal sections were observed, and the time evolutions of the fast radiation powers with the plasma center sight lines were measured by absolute extra ultraviolet silicon photodiode (AXUVD) at port 3.5U (close to the HAS antenna) and port 8O (close to the PA antenna). These fast radiation powers were synchronized on low-frequency modulation with each other, and the modulations were caused by magnetic axis sweeping to decrease the concentration of the local heat load to the divertor plates. On the other hand, the spike frequencies of these fast radiations were not always synchronized with each other, and the spike frequencies of impurity lines (CIII and FeXVI) were not always synchronized with the fast radiation powers, either. In this plasma, electron temperature with normalized minor radius $\rho \sim 0.8$ was approximately a few hundred eV, and iron and carbon impurities were ionized at the plasma edge. The experimental results suggest that mainly radiation spikes are produced around the plasma edges of local toroidal sections and impurity accumulation is negligible on the long-pulse operation with $\tau_d \sim 19$ min. Comparing the radiation spikes of the 8O port (d) with that of 3.5U port (e), the spike frequency found near the PA antenna was much larger than that found near the HAS antenna, and there were many heating power degradation events by interlocks for the PA antenna. The reflection ratio of the heating power supplied the PA antenna was over at many times. In the previous long-pulse discharge, the frequency of these spikes with the CIII line was not so much larger than that with $P_{RF} \sim 1$ MW, and the spike frequency was increased with increased divertor heat loads and increased plasma heating power from 0.5 MW to 1 MW. By increasing the edge plasma temperature and the divertor heat load with the RF heating power, the reason for the plasma termination was changed from radiation collapse caused by an impurity penetration for iron at the plasma edge to the increase in electon density. The unintended heating power decrease by the interlcok for ICH made the sustainable density small, and the time scale of the plasma termination was extended from 0.2 s by impurity contamination to a few seconds by exceeding the sustainable density. On the steady-state operation, low impurity production and stable plasma heating were achieved using the HAS antenna while it was necessary to decease the interlock events and the temperature of the antenna protector for the PA antenna.

D. Decreased wall-recycling and divertor heat load on long-pulse discharges

Figure 5 shows time evolutions of n_e, He fueling rate (Γ_{He}) and RF heating power (P_{RF}) on the two long-pulse operations, and in the relatively short-pulse discharge with $\tau_d \sim 6$ min (#113145) He fueling is carried out using a mass-flow controller (MFC, a controllable fueling rate < 2 Pa m^3/s) by a proportional feedback method (P method) between n_e and the preprogrammed target value. Except for the plasma startup phase, Γ_{He} gradually decreased in 200 s, and then Γ_{He} reached $\sim$0.036 Pa m^3/s, which is similar to the slow leak rate for the MFC. On the longer-pulse plasma discharge, it seemed necessary to control the He-fueling rate ($\Gamma_{He} < 0.036$ Pa m^3/s), and a piezoelectric valve to control the very small Γ_{He} was used in the long-pulse discharge with $\tau_\delta \sim 19$ min (#117208). He fueling using the valve adopted the P method that was previously used in a long-pulse

discharge with $\tau_d \sim 54$ min, $n_e < 0.5 \times 10^{19}$ m^{-3} and $P_{RF} \sim 0.5$ MW,[3] and the n_e was well controlled using the P method. On higher-performance plasma with $n_e \sim 1 \times 10^{19}$ m^{-3}, T_{e0} greater than a few keV and $P_{RF} \sim 1$ MW (#117208), the He fueling rate was overestimated by the P method in 700 s, and the electron density gradually increased after 700 s. The P method is useful to achieve a constant electron density with a small perturbation for the target density; it is assumed that the wall-recycling rate during the plasma duration is constant. In Figure 5(d), the He wall-recycling rate estimated from the rate of decreasing in n_e was consistent with the exhausting rate for active pumping speed around $t = 815$–835 s (the phase II). The hydrogen fueling to keep the minority ratio was carried out by super-sonic gas puffing (SSGP) at fueling rates less than 0.01 Pa m^3/s, and there was no active fueling except wall-recycling included from the divertor in phase II. That suggests that the wall-recycling ratio was negligible around 820 s in phase II; it will be necessary to improve a particle fueling method to adopt electron density with the time evolution for the wall-recycling in the long-pulse discharge.

Figure 6 shows the removed divertor heating power in various toroidal sections for long-pulse operations with $\tau_d > 430$ s. The power removed from the divertor plates was calculated from the divertors' cooling-water temperature. In order to estimate the average power removed from the divertor plates, the summation of the total removed energy was divided by the plasma duration time, and the energy until the divertor temperature reached the initial temperature before plasma discharge was summed. ECH was carried out at port 1.5, 2, and port 9.5 as direct electron heating, and ICRF power was supplied at port 3.5 with the HAS antenna at dipole phase and at port 7.5 with the PA antenna at monopole phase. Comparing the unbalanced removed power using HAS + PA antenna with that using HAS antenna, the removed power was localized around the heating port using the PA antenna. In the case using the HAS antenna, the

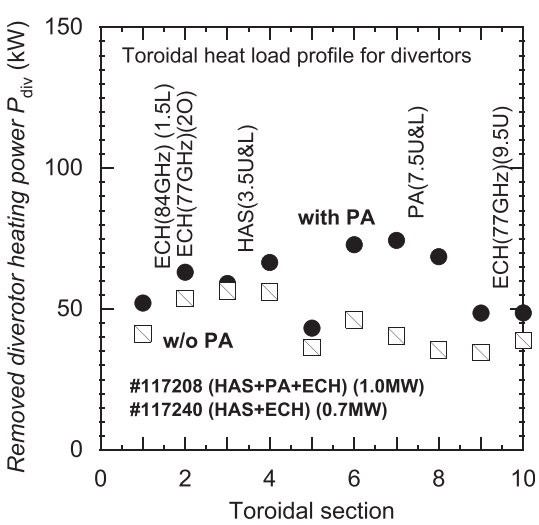

FIG. 6. Amounts of power removed from the divertor plates (P_{div}) in various toroidal sections for two heating operations with the PA + HAS antenna (#117208) and the HAS antenna alone (#117240), are shown. When the PA antenna was used, the removed power was locally increased around the PA antenna.

unbalanced removed heating power around the HAS antenna was much smaller than that using the PA antenna. Energetic particles are easily accelerated on the outside of the LCFS in front of the ICRF antenna, and these particles locally impact the specific divertor plates to which magnetic field line connects in front of the ICRF antenna.[4] The particle acceleration in front of the ICRF antenna is related to the RF sheath potential, and the RF sheath potential around the ICRF antenna for the HAS antenna seems to be smaller than that for the PA antenna. For heat balance on long-pulse discharge with the τ_d of 19 min, an amount of 64% for heating power went to the divertor plates using the HAS+PA antenna, and the power ratio to the divertor only using the HAS antenna for ICH was approximately the same as that using the HAS+PA antenna. Considering the higher dipole-phase heating efficiency of the HAS antenna than the PA antenna with phasing monopole, parasitic heating loss for the PA antenna with low wavenumber ($k_{\parallel} \sim 0$ m^{-1}) was caused by the accelerated energetic particles in front of ICRF antenna. The amount of radiation power measured by bolometer, which was installed at close HAS antenna, was approximately 18% using the HAS + PA antenna, and the impurity accumulation for the core plasma was not different between two kinds of ICRF antennas.

IV. SUMMARY AND DISCUSSION

In order to achieve high-performance steady-state operation using ICH in the LHD, long-pulse experiments using two kinds of ICRF antennas have been performed, and it is necessary to prepare the calculation framework including wave propagation with an actual antenna and vacuum vessel model to predict the RF sheath effect using COMSOL. The calculation framework for ICH in LHD is under construction, and we have to reduce the computational resources required to include the Faraday screen and antenna protector with a hot plasma tensor to reveal parasitic heating losses in front of the ICRF antennas. The HAS antenna was designed to decrease parasitic losses associated with energetic particle and RF sheath potential around the ICRF antenna, and, with several real-time feedback controls for impedance matching and maintaining constant power and antenna phase, a long-pulse discharge with $\tau_d \sim 19$ min, $n_e \sim 1 \times 10^{19}$ m^{-3}, electron and ion temperature of 2 keV were achieved. Hydrogen fueling by SSGP effectively reduced flashes around the PA antenna, and the heating power for the PA antenna was easily shunted to nearby divertor plates with low hydrogen concentrations. That power for the HAS antenna was smaller than that for the PA antenna, and the parasitic losses using the HAS antenna, which was associated with energetic particle acceleration in front of the ICRF antenna and weak plasma production by RF sheath, was smaller than that using the PA antenna. The particle fueling rate with $\tau_d > 700$ s was smaller than the assumption from the rate of long-pulse discharge with $\tau_d \sim 54$ min, $n_e \sim 0.4 \times 10^{19}$ m^{-3}, and $P_{RF} \sim 0.5$ MW. The local heat load to the divertor plate, the first wall and the hot spot temperature associated with parasitic losses were increased as the minority ratio of hydrogen decreased, and the heated first wall was one of the

possibilities for the decreased He fueling ratio at $\tau_d > 700$ s. The HAS antenna could reduce those temperature and local hot spots of antenna protectors; then, the long-pulse discharge with higher heating power might be more easily supplied than that using the PA antenna. For the HAS antenna, the heating efficiency of the monopole phase, which was consistent with the heating efficiency using the PA antenna, was smaller than that of the dipole phase, and the heating efficiency seemed to be related to its operation in toroidal phases. We could not reveal the local hot-spot temperatures between the field-aligned effect and the dipole operation on the steady-state operation, because the ICH operation with higher heating efficiency was usually adopted on long-pulse discharges. In the future, we want to compare the local hot spots in relative long-pulse discharge ($\tau_d \sim 10$ min) at monopole and dipole phases, and have a plan to perform a field-aligned poloidal array antenna experiment.

ACKNOWLEDGMENTS

Thanks are due to S. Shiraiwa (MIT, USA), O. Meneghini (GA, USA) and T. Watanabe (NIFS, Japan) for improving the framework of wave-propagation with the three-dimensional magnetic field configuration and cold plasma model. This work was supported by the LHD projects (NIFS12ULRR703, 801) and Japan/U.S. cooperation in fusion research and development in steady-state operation.

[1]A. Komori, H. Yamada, S. Sakakibara, O. Kaneko, K. Kawahata, T. Mutoh, N. Ohyabu, S. Imagawa, K. Ida, Y. Nagayama, T. Shimozuma, K. Y. Watanabe, T. Mito, M. Kobayashi, K. Nagaoka, R. Sakamoto, N. Yoshida, S. Ohdachi, N. Ashikawa, Y. Feng, T. Fukuda, H. Igami, S. Inagaki, H. Kasahara, S. Kubo, R. Kumazawa, O. Mitarai, S. Murakami, Y. Nakamura, M. Nishiura, T. Hino, S. Masuzaki, K. Tanaka, K. Toi, A. Weller, M. Yoshinuma, Y. Narushima, N. Ohno, T. Okamura, N. Tamura, K. Saito, T. Seki, S. Sudo, H. Tanaka, T. Tokuzawa, N. Yanagi, M. Yokoyama, Y. Yoshimura, T. Akiyama, H. Chikaraishi, M. Chowdhuri, M. Emoto, N. Ezumi, H. Funaba, L. Garcia, P. Goncharov, M. Goto, K. Ichiguchi, M. Ichimura, H. Idei, T. Ido, S. Iio, K. Ikeda, M. Irie, A. Isayama, T. Ishigooka, M. Isobe, T. Ito, K. Itoh, A. Iwamae, S. Hamaguchi, T. Hamajima, S. Kitajima, S. Kado, D. Kato, T. Kato, S. Kobayashi, K. Kondo, S. Masamune, Y. Matsumoto, N. Matsunami, T. Minami, C. Michael, H. Miura, J. Miyazawa, N. Mizuguchi, T. Morisaki, S. Morita, G. Motojima, I. Murakami, S. Muto, K. Nagasaki, N. Nakajima, Y. Nakamura, H. Nakanishi, H. Nakano, K. Narihara, A. Nishimura, H. Nishimura, K. Nishimura, S. Nishimura, N. Nishino, T. Notake, T. Obana, K. Ogawa, Y. Oka, T. Ohishi, H. Okada, K. Okuno, K. Ono, M. Osakabe, T. Osako, T. Ozaki, B. J. Peterson, H. Sakaue, M. Sasao, S. Satake, K. Sato, M. Sato, A. Shimizu, M. Shiratani, M. Shoji, H. Sugama, C. Suzuki, Y. Suzuki, K. Takahata, H. Takahashi, Y. Takase, Y. Takeiri, H. Takenaga, S. Toda, Y. Todo, M. Tokitani, H. Tsuchiya, K. Tsumori, H. Urano, E. Veshchev, F. Watanabe, T. Watanabe, T. H. Watanabe, I. Yamada, S. Yamada, O. Yamagishi, S. Yamaguchi, S. Yoshimura, T. Yoshinaga, and O. Motojima, Proc. Nucl. Fusion **49**, 104015 (2009).

[2]T. Mutoh, R. Kumazawa, T. Seki, K. Saito, H. Kasahara, Y. Nakamura, S. Masuzaki, S. Kubo, Y. Takeiri, T. Shimozuma, Y. Yoshimura, H. Igami, T. Watanabe, H. Ogawa, J. Miyazawa, M. Shoji, N. Ashikawa, K. Nishimura, M. Osakabe, K. Tsumori, K. Ikeda, K. Nagaoka, Y. Oka, H. Chikaraishi, H. Funaba, S. Morita, M. Goto, S. Inagaki, K. Narihara, T. Tokuzawa, R. Sakamoto, T. Morisaki, B. J. Peterson, K. Tanaka, H. Nakanishi, M. Nishiura, T. Ozaki, F. Shimpo, G. Nomura, C. Takahashi, M. Yokota, Y. P. Zhao, J. G. Kwak, S. Murakami, H. Okada, H. Yamada, K. Kawahata, N. Ohyabu, O. Kaneko, K. Ida, Y. Nagayama, K. Y. Watanabe, N. Noda, A. Komori, S. Sudo, and O. Motojima, in *Proceedings of the 21st IAEA Conference on Fusion Energy*, Chengdu, China EX/P1-14 (IAEA, Vienna, 2006).

[3]H. Kasahara, T. Seki, K. Saito, R. Kumazawa, S. Kubo, T. Shimozuma, Y. Yoshimura, H. Igami, T. Notake, Y. Nakamura, J. Miyazawa, and K. Tanaka, Fusion Eng. Des. **83**, 253–255 (2008).

[4]H. Kasahara, T. Seki, K. Saito, R. Kumazawa, T. Mutoh, F. Shimpo, and G. Nomura, Plasma Fusion Res. **5**, S2090 (2010).

[5]T. Mutoh, S. Masuzaki, R. Kumazawa, T. Seki, K. Saito, Y. Nakamura, S. Kubo, Y. Takeiri, T. Shimozuma, Y. Yoshimura, H. Igami, K. Ohkubo, T. Watanabe, H. Ogawa, J. Miyazawa, M. Shoji, N. Ashikawa, K. Nishimura, M. Sakamoto, M. Osakabe, K. Tsumori, K. Ikeda, H. Chikaraishi, H. Funaba, S. Morita, M. Goto, T. Tokuzawa, N. Takeuchi, F. Shimpo, G. Nomura, C. Takahashi, M. Yokota, Y. P. Zhao, J. G. Kwak, H. Yamada, K. Kawahata, N. Ohyabu, O. Kaneko, K. Ida, Y. Nagayama, N. Noda, A. Komori, S. Sudo, and O. Motojima, Phys. Plasmas **13**, 056118 (2006).

[6]R. Kumazawa and K. Saito, Annual report of NIFS, plasma collapse by external injection Fe pellet, Report No. S11, 2008.

[7]F. Waelbroeck, J. Winter, G. Esser, B. Giesen, L. Konen, V. Philipps, U. Samm, J. Schluter, P. Weinhold, and the TEXTOR Team, Plasma Phys. Controlled Fusion **31**, 185 (1989).

[8]M. Bures, H. Brinkschulte, J. Acqunot, K. D. Fawson, A. Kaye, and J. A. Tagle, Plasma Phys. Controlled Fusion **30**, 149 (1988).

[9]M. Bures, J. J. Jacquinot, M. F. Stamp, D. D. R. Summers, D. F. H. Start, and T. Wade, Nucl. Fusion **32**, 1139 (1992).

[10]J. Menard, R. Majeski, R. Kaita, M. Ono, T. Munsat, D. Stutman, and M. Finkenthal, Phys. Plasmas **6**, 2002 (1999).

[11]L. Colas, L. Costanzo, C. Desgranges, S. Brémond, J. Bucalossi, G. Agarici, V. Basiuk, B. Beaumont, A. Bécoulet, and F. Nguyen, Nucl. Fusion **43**, 1–15 (2003).

[12]P. Jacquet, L. Colas, M.-L. Mayoral, G. Arnoux, V. Bobkov, M. Brix, P. Coad, A. Czarnecka, D. Dodt, F. Durodie, A. Ekedahl, D. Frigione, M. Fursdon, E. Gauthier,M. Goniche, M. Graham, E. Joffrin, A. Korotkov, E. Lerche, J. Mailloux, I. Monakhov, C. Noble, J. Ongena, V. Petrzilka, C. Portafaix, F. Rimini, A. Sirinelli, V. Riccardo, Z. Vizvary, A. Widdowson, K.-D. Zastrow, and JET EFDA Contributors, Nucl. Fusion **51**, 103018 (2011).

[13]L. Colas, S. Heuraux, S. Bremond, and G. Bosia, Nucl. Fusion **45**, 767–782 (2005).

[14]D. A. D'ippolito and J. R. Myra, J. Nucl. Mater. **415**, S1001 (2011).

[15]M. L. Garrett and S. J. Wukitch, Fusion Eng. Des. **87**, 1570 (2012).

[16]S. J. Wukitch, D. Brunner, M. L. Garrett, B. Labombard, C. Lau, Y. Lin, B. Kipschultz, R. Ochoukov, M. L. Reinke, J. L. Terry, D. Whyte, and the Alcator C-Mod Team, "Evaluation of a field aligned ICRF antenna in Alcator C-Mod," in *Proceedings of the 24th IAEA Fusion Energy Conference, San Diego, CA*, (IAEA, Vienna, 2012).

[17]M. Brambilla, *Kinetic Theory of Plasma Waves* (Oxford, 1998).

[18]S. Shiraiwa, O. Meneghini, R. Parker, A. E. Schmidt, S. Scott, M. Greenwald, A. E. Hubbard, J. Hughes, Y. Ma, Y. Podpaly, E. Rice, G. Wallace, J. R. Wilson, S. M. Wolf, and Alcator C-Mod Group, Phys. Plasmas **18**, 080705 (2011).

[19]See http://www.comsol.com for COMSOL multiphysics.

[20]K. Saito, R. Kumzawa, C. Takahashi, M. Yokota, H. Takeuchi, T. Mutoh, T. Seki, F. Shimpo, G. Nomura, T. Watari, A. Komori, Y. Torii, J. S. Yoon, J. G. Kwak, Y. Zaho, and LHD Experimental Group, Fusion Eng. Des. **81**, 2837–2842 (2006).

[21]R. Kumazawa, T. Mutoh, T. Seki, T. Watari, K. Saito, Y. Torii, F. Shimpo, G. Nomura, M. Yokota, A. Kato, D. A. Hartmann, Y. Zhao, A. Fukuyama, H. Okada, K. Ohkubo, M. Sato, S. Kubo, T. Shimozuma, H. Idei, Y. Yoshimura, T. Notake, Y. Takita, S. Kobayashi, S. Itoh, Y. Mizuno, O. Kaneko, Y. Takeiri, Y. Oka, K. Tsumori, M. Osakabe, K. Ikeda, S. Yamamoto, T. Kawamoto, E. Asano, N. Ohyabu, K. Kawahata, A. Komori, H. Yamada, K. Akaishi, N. Ashikawa, M. Emoto, H. Funaba, M. Goto, K. Ida, S. Inagaki, N. Inoue, M. Isobe, A. Krasilnikov, S. Masuzaki, T. Minami, J. Miyazawa, T. Morisaki, S. Morita, S. Murakami, S. Muto, Y. Nakamura, Y. Nagayama, H. Nakanishi, K. Narihara, Y. Narushima, K. Nishimura, N. Noda, T. Kobuchi, S. Ohdachi, T. Ozaki, B. J. Peterson, A. Sagara, S. Sakakibara, R. Sakamoto, H. Sasao, M. Sasao, K. Sato, M. Shoji, H. Suzuki, K. Tanaka, K. Toi, T. Tokuzawa, I. Yamada, S. Yamaguchi, M. Yokoyama, K.-Y. Watanabe, T. Watanabe, K. Matsuoka, K. Itoh, S. Sudo, K. Yamazaki, Y. Hamada, O. Motojima, M. Fujiwara, and LHD Experimental Group, Rev. Sci. Instrum. **70**, 2665–2673 (1999).